THE ASTROPHYSICAL JOURNAL, 282:245–255, 1984 July 1

SPECTRAL VARIABILITY IN EARLY-TYPE BINARY X-RAY SYSTEMS

RICHARD MCCRAY[1] AND TIMOTHY R. KALLMAN
NASA/Goddard Space Flight Center
JOHN I. CASTOR
Lawrence Livermore National Laboratory
AND
GORDON L. OLSON
Los Alamos National Laboratory
Received 1983 November 14; accepted 1984 January 13

ABSTRACT

We present theoretical models for the ionization of trace elements in a strong stellar wind by a compact binary X-ray source and for the resulting orbital phase dependence of the emergent soft X-ray spectra and the profiles of ultraviolet resonance lines. Model results agree qualitatively with the X-ray and ultraviolet spectra of the system 4U 0900−40/HD 77581 and explain the suppression of the absorption profiles of the Si IV λ1394 and C IV λ1548 lines when the X-ray source is in front of the star. The model predicts that the absorption profiles of the N V λ1239 and O VI λ1032 lines will be enhanced rather than suppressed during this orbital phase. We predict phase-dependent linear polarization in the resonance line profiles. We discuss how future observations of these phase dependent effects in early-type binary X-ray systems may be used to investigate the dynamics of stellar winds and their interactions with the X-ray source.

Subject headings: polarization — stars: individual — stars: winds — X-rays: binaries — X-rays: spectra

I. INTRODUCTION

Early-type giant and supergiant stars have strong stellar winds, with mass loss rates in the range $\dot{M} \approx 10^{-8}$ to $\approx 10^{-5}$ $M_\odot$ yr^{-1} and terminal velocities in the range $\approx$500 to $\approx$3000 km s^{-1} (Conti and McCray 1980). The winds are probably driven by resonance scattering of the stellar radiation by ions in the wind, but this interaction is not fully understood. In particular, the theoretical models do not accurately account for the ionization of trace elements in the wind or for the details of the observed resonance line shapes and strengths, and they do not explain the observations of soft X-ray emission from such stars, which is probably produced by shocks or instabilities in the wind (Lucy and White 1980).

Several galactic OB stars have compact X-ray source companions in close binary orbits. In such systems the winds can have sufficient column density to cause soft X-ray absorption variations with orbital phase (Buff and McCray 1974). In turn, a luminous X-ray source can substantially modify the ionization of trace elements in the wind, causing a phase dependence of the ultraviolet P Cygni type line profiles formed by these trace elements (Hatchett and McCray 1977). Observations have confirmed the existence of phase dependences in the X-ray and UV spectra from a few of the X-ray binaries with OB supergiant companions (e.g., Dupree *et al.* 1978, 1980; Hammerschlag-Hensberge *et al.* 1980; van der Klis *et al.* 1982; Kallman and White 1982; and references therein). These observations provide a probe of the density and ionization structure in the winds of these systems.

A compact binary X-ray source in a stellar wind is not only a passive probe of the wind; it is also an active probe of the physical mechanism for accelerating the wind. The X-ray emission can modify the dynamics of the wind directly through radiation pressure and indirectly through changing the ionization of trace elements and, hence, the coupling of the stellar radiation to the wind (e.g., MacGregor and Vitello 1982; Friend and Castor 1982; Fransson and Fabian 1982). These effects are complex and poorly understood.

In principle, we should be able to gain a satisfactory understanding of these systems by constructing theoretical models for the ionization structure and dynamics of the winds and calculating the resulting orbital variations of their X-ray and UV spectra that may be compared to the observations. In practice, this goal is distant, because we do not even understand the structure and dynamics of stellar winds of single OB stars, much less of binary X-ray sources, and the properties of the stellar winds are sensitive to many physical parameters that are not well known. For single stars these include the wind density (mass loss rate, velocity law) and ionization (which is affected by the diffuse X-ray spectrum in the wind). For binary systems, additional uncertainties arise from intrinsic variability of the X-ray source and from lack of knowledge of the soft X-ray spectrum (which strongly affects the ionization of trace elements in the wind).

In this paper we consider a more idealized model, in which the dynamics of the stellar wind are not affected by the X-ray source, so that the wind's velocity and density distributions are assumed to be spherically symmetric and identical to what they would be in the absence of the X-ray source. However, we do calculate quantitative models for the ionization of the wind and for the variations of the X-ray and UV spectra resulting from the orbital motions of the X-ray source for the example of 4U 0900−40/HD 77581 (Vela X-1), the best observed such system. In § II we describe a heuristic model for the structure and ionization of a stellar wind around an isolated O star. In § III we describe the ionization structure of a stellar wind with an embedded X-ray source and the resulting orbital variations of the X-ray spectrum, and in § IV

[1] On leave from JILA and Department of Astrophysics, University of Colorado.

we describe the variations in the UV resonance line profiles. In § V we compare these model results with present observations of 4U 0900−40/HD 77581, we discuss the limitations of the model, and we discuss what may be learned from further observations of this and other such systems.

II. THE UNDISTURBED STELLAR WIND

As shown by Olson and Castor (1981), the detailed calculation of the ionization equilibrium of several ions of several elements in the expanding winds of normal O and B type stars is quite complex. Besides direct photoionization from the stellar flux, diffuse radiation from the optically thick wind also contributes significantly to the photoionization rates. Trace amounts of ions with large ionization potentials, such as O VI, are produced by Auger ionization from X-rays produced in the winds of normal stars (Olson 1978; Cassinelli and Olson 1979).

In the spirit of approximation adopted for this paper, we shall try to infer the background stellar wind conditions from observed spectra rather than attempt to construct a detailed wind model, as was done by Olson and Castor (1981). In this way we include the effects of the observed soft X-ray emission from isolated OB stars. The background ion fractions and ionization rates in the undisturbed stellar wind have been estimated in order to fit the theoretical profiles to the observed profiles according to the method suggested by Castor and Lamers (1979). The optical depth along the radius, R, from the stellar center is written as a function of the velocity:

$$\tau(w) = T(1+\gamma)(1-w_0)^{-1-\gamma}(1-w)^{\gamma}\,, \qquad (1)$$

where $w(R) = v(R)/v_\infty$ is the radial wind velocity normalized to the terminal velocity v_∞, $w_0 = w(R_*)$ is the wind velocity at the stellar continuum photosphere, and T and γ are adjustable parameters. We assume that the wind velocity is spherically symmetric about the primary and is given by

$$w(R) = 1 - 0.98R_*/R\,, \qquad (2)$$

which corresponds to $w_0 = 0.02$ and $\beta = 1$ in the notation of Castor and Lamers. Equation (2) gives good results for most O star P Cygni line profiles.

The profiles of Si IV and C IV in HD 77581 have been observed at several orbital phases (Dupree *et al.* 1980). Although the observed profiles do not agree in detail with the theoretical profiles in the atlas of Castor and Lamers (1979), fits of the profiles observed during X-ray eclipse ($\phi = 0$) provide an estimate of the distribution of scattering ions in the wind of HD 77581 in the absence of ionization by the compact X-ray source. The parameters of these fits are given in Table 1.

Unfortunately, observations of the N V and O VI resonance lines of HD 77581 are not available. Therefore, we assume that the undisturbed wind profiles are the same as those of the star κ Ori (B0.5 Ia), which is very similar to HD 77581 but does not have a compact companion. Gathier, Lamers, and Snow (1981) have analyzed *Copernicus* spectra of κ Ori and have fitted theoretical line profiles using equation (1). The parameters of their fits, which will be adopted as appropriate for HD 77581, are given in Table 1.

In order to deduce the ion fractions, the radial optical depth in equation (1) must be equated to the Sobolev radial optical depth:

$$\tau_\lambda(R) = \frac{\pi e^2}{m_e c}\,\lambda_0\, f_\lambda\, n_i^{\,j}\left(\frac{dv}{dR}\right)^{-1}\,, \qquad (3)$$

TABLE 1

PROFILE PARAMETERS FOR UV RESONANCE LINES

Line	λ (Å)	T	γ	A_i
C IV	1548.19	20	2	3.3(−4)
N V	1238.81	1	0.5	9.1(−5)
O VI	1031.93	2	0.5	6.6(−4)
Si IV	1393.76	6	2	3.3(−5)

where λ_0 is the rest wavelength of the transition, f_λ is its oscillator strength, and dv/dR is the radial velocity gradient of the wind at the surface where $\lambda = \lambda_0[1 - (v/c)]$. The density, $n_i^{\,j}$, of ions of element i in charge state j, can be related to other quantities by using mass conservation in spherical symmetry:

$$n_i^{\,j}(R) = n(R)A_i g_i^{\,j} = \dot{M}A_i g_i^{\,j}/[4\pi R^2 \mu v(R)]\,, \qquad (4)$$

where $n(R)$ is the atomic density, A_i is the element abundance relative to hydrogen, $g_i^{\,j}$ is the ion fraction relative to the element, and μ is the mean molecular weight. Combining equations (1)–(4) will specify the ionization fraction as a function of radius as determined from the fitted profiles.

Because the compact X-ray source provides an additional source of photoionization, it is convenient to determine an effective ionization rate for the undisturbed wind. Balancing recombinations and ionizations gives

$$n_i^{\,j+1} n_e\, \alpha_i^{\,j+1}(T_e) = n_i^{\,j}\zeta_i^{\,j}\,, \qquad (5)$$

where n_e and T_e are the electron density and temperature, α (cm^3 s^{-1}) is the recombination rate coefficient, and ζ is the effective ionization rate.

We assume that HD 77581 has a radius $R_* = 35\ R_\odot$, a wind temperature $T_e = 0.9T_{\rm eff} = 23{,}000$ K, and a terminal wind velocity $v_\infty = 1700$ km s^{-1}. Since most of the carbon and silicon are in the forms C V and Si V, equations (1)–(5) imply that

$$\zeta(\text{Si IV}) = 0.073\dot{M}_{-6}{}^2[(1-w)^2x^4w^2dw/dx]^{-1}\ \text{s}^{-1} \qquad (6)$$

and

$$\zeta(\text{C IV}) = 0.12\dot{M}_{-6}{}^2[(1-w)^2x^4w^2dw/dx]^{-1}\ \text{s}^{-1}\,, \qquad (7)$$

where $\dot{M}_{-6}$ is the mass loss rate in units of $10^{-6}\ M_\odot$ yr^{-1} and $x = R/R_*$ is the distance from the primary in units of the radius of the stellar photosphere. These "background" ionization rates in the unperturbed stellar wind will be added to the rates produced by the compact X-ray source.

We infer the ionization fractions of N V and O VI from the line profiles of κ Ori, using equations (1)–(4), the stellar parameters and those in Table 1. The results are:

$$g(\text{N V}) = 0.011\dot{M}_{-6}{}^{-1}[1 - (0.98/x)]x^{-1/2} \qquad (8)$$

and

$$g(\text{O VI}) = 0.0041\dot{M}_{-6}{}^{-1}[1 - (0.98/x)]x^{-1/2}\,. \qquad (9)$$

Auger ionization produces all of the O VI seen in the winds of the O and B type stars and the N V seen in early B type stars (Cassinelli and Olson 1979). Auger ionization couples several ionization stages, making it difficult to specify a meaningful effective ionization rate. Therefore, since most of the nitrogen and oxygen are in the forms N IV and O IV, we take the results of equations (8) and (9) to represent the lower bounds of the abundances of N V and O VI that will occur in the wind.

III. IONIZATION AND X-RAY TRANSFER

An accurate description of the ionization and heating produced by an X-ray source in a stellar wind is complicated both by the physics of X-ray transfer and by the binary geometry. X-rays have the property that they can completely ionize all abundant trace elements, and that they can heat gas to temperatures greater than 10^7 K. The binary geometry requires a two-dimensional solution of the coupled transfer and ionization heating problem. In this section we describe our technique for modeling the effects of a compact X-ray source embedded in a stellar wind and discuss some of the important features of these models.

An understanding of the ionization structure of the X-ray illuminated wind can be gained by considering a simplified model. If the effects of background ionization due to the stellar radiation field and other sources are neglected and the wind is assumed to be optically thin, then the ionization state and temperature of the gas at any point depend only on the X-ray source spectrum and the ionization parameter, $\xi = L_x/nr^2$, where L_x is the total X-ray luminosity, r is the distance from the X-ray source, and $n(r)$ is the local gas density (Tarter, Tucker, and Salpeter 1969). If the wind has a spherically symmetric density distribution, $n(R) \approx R^{-2}$ (steady flow at constant velocity), the surfaces of constant ξ, and hence of constant ionization and temperature, are either spheres surrounding the X-ray source or open surfaces surrounding the primary (Hatchett and McCray 1978). Generally, the geometry of these surfaces can be characterized by the dimensionless parameter

$$q = \xi n_x D^2/L_x = R^2 v(R)/[r^2 v(D)]\,, \qquad (10)$$

where n_x is the wind density at the X-ray source and D is the orbital separation. The surface $q = 1$ determines the boundary between the open ($q < 1$) and closed ($q > 1$) surfaces. Furthermore, Hatchett and McCray showed that these conclusions are essentially unchanged when X-ray absorption effects are considered.

In the region of the wind where ionization and heating are due both to X-rays and to background ionization by the stellar radiation field and other sources, an accurate description of the state of the gas requires the construction of more detailed models. In the absence of X-rays the background ionization depends on R, the distance to the primary, and the dependence of the gas state on both X-rays and background ionization breaks the simple ξ-scaling arguments described above. We have modeled the ionization and temperature structure produced by a compact X-ray source in a stellar wind by solving the coupled ionization equilibrium, thermal equilibrium, and radiative transfer equations along a series of rays from the X-ray source. The temperature, ion abundances, and radiation field are computed as functions of distance along each ray using the X-ray transfer code described by Kallman and McCray (1982). This code includes the effects of a great number of atomic processes in a gas consisting of all ion stages of the abundant elements H, He, C, N, O, Ne, Si, S, and Fe. The radiative transfer equation is solved in a simplified single-stream approximation, in which the diffuse emission by the gas at any point is assumed to be produced by material with a spherically symmetric distribution centered on the X-ray source. We find that 12 rays evenly distributed in polar angle with respect to the line of centers are sufficient to provide an accurate interpolation of the ionization structure between the rays.

Input parameters for the model include the X-ray source luminosity and spectral shape. We use values appropriate to 4U 0900−40 (Becker *et al.* 1978), consisting of a 20 keV bremsstrahlung spectrum with a total luminosity $L_x = 10^{36}$ ergs s^{-1}. The gas density at any point in the wind is determined by the total mass loss rate of $\dot{M} = 4 \times 10^{-6}\ M_\odot\ \mathrm{yr}^{-1}$, based on examination of UV line profiles during X-ray eclipse (Dupree *et al.* 1980) and an assumed steady spherically symmetric flow with velocity law given by equation (2) and $v_\infty = 1700$ km s^{-1}. The curves of constant ionization parameter are shown in Figure 1, where $\zeta = \log_{10} \xi$.

The abundances of ions with threshold energies less than 100 eV are affected by the copious UV flux from the primary star. We model the ionization due to this component of the radiation by adding to the flux at each point in the wind a blackbody field with temperature $T_* = 26{,}000$ K, diluted according to the distance from the primary. For Si IV and C IV the background ionization rates (eqs. [6] and [7]) are added to the X-ray photoionization rates. For N V and O VI we take the background ionization fractions (eqs. [8] and [9]) as lower bounds to the actual ionization fractions when the X-ray flux is weak. In order to ensure that the ionization structure of other elements far from the X-ray source approximates the true background ionization in the wind we have imposed an artificial lower limit on the gas temperature of 90% of the blackbody temperature, i.e., $T_{\min} = 23{,}000$ K (Klein and Castor 1978; Gathier, Lamers, and Snow 1981).

The ionization structure of the stellar wind is illustrated in Figures 2*a*–2*d*, which show surfaces of constant fractional ion abundance, g_i^j, for the ions C IV, Si IV, N V, and O VI. Close to the X-ray source these surfaces closely resemble spheres, as shown by Hatchett and McCray (1977). The X-rays clearly suppress the abundances of Si IV and C IV throughout most of the half-space occupied by the X-ray source. Outside of this region other ionization processes become important, and on the far side of the primary the abundances are unaffected

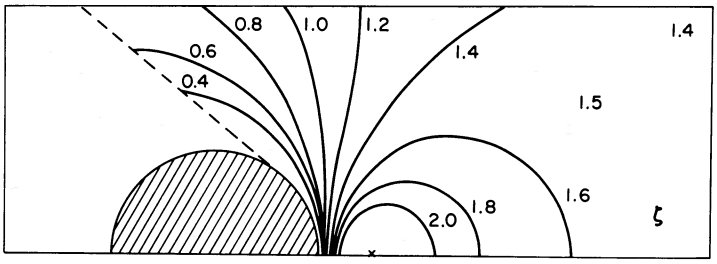

FIG. 1.—Contours of constant ionization parameter, $\xi = L_x/nr^2$ for the 4U 0900−40/HD 77581 system. The curves are labeled by $\zeta = \log_{10} \xi$.

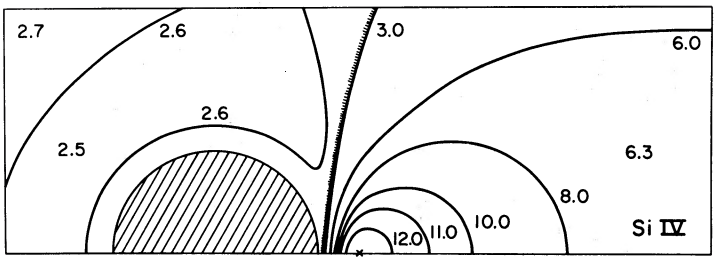

FIG. 2a

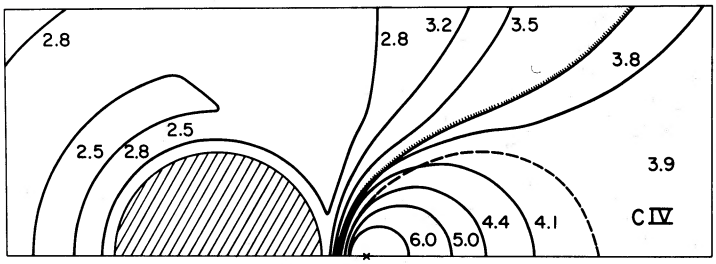

FIG. 2b

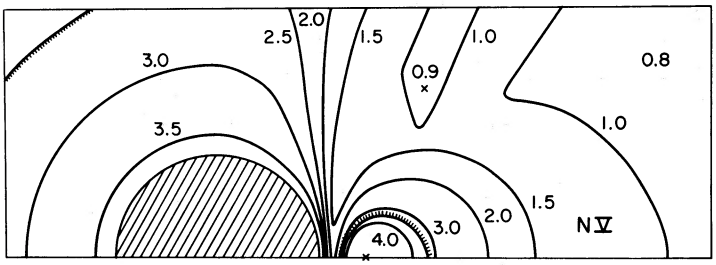

FIG. 2c

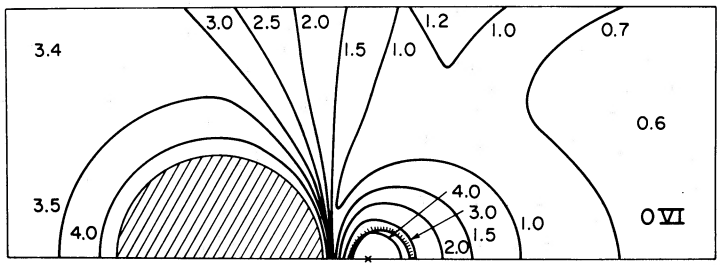

FIG. 2d

FIG. 2.—(*a*) Contours of constant fractional abundance, g_i^j, for Si IV. The curves are labeled by $(-\log_{10} g_i^j)$. The curve with hatch marks indicates the boundary where the resonance line opacity $\tau_\lambda = 1$, separating the optically thick (*hatched side*) from the optically thin (*solid side*) zones. (*b*) Same as Fig. 2*a* but for C IV. The dashed curve represents $\tau_\lambda = \frac{1}{2}$. (*c*) Same as Fig. 2*a* but for N V. (*d*) Same as Fig. 2*a* but for O VI.

by the X-ray source. Since C IV and Si IV are less ionized than the dominant ions (C V and Si V), their abundances are suppressed near the X-ray source and increase monotonically with distance from the X-ray source. Close to the primary star the high wind densities suppress the destruction of Si IV and C IV, causing their surfaces of constant abundance to partially wrap around the primary.

In contrast, N V and O VI are more ionized than the dominant ions (N IV, O IV, and O V), and their abundances (Figs. 2*c* and 2*d*) are *enhanced* by more than two orders of magnitude throughout most of the half-space containing the X-ray source as a result of photoionization of the more abundant ions. The enhancement of O VI illustrates the penetrating power of the 1 keV X-rays responsible for the production of this ion via *K*-shell photoionization followed by Auger emission. Close to the X-ray source the abundances of N V and O VI are suppressed by ionization to higher stages, and the surfaces of constant ionization are nearly spherical.

Our model calculations also yield the X-ray spectra emerging from the various rays from the source, displayed in Figure 3. These spectra illustrate the orbital variations that a distant observer will see as a result of the changing column density

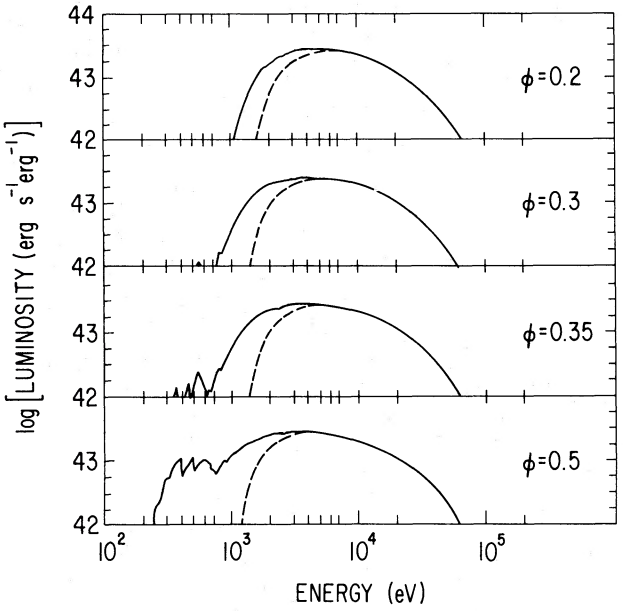

FIG. 3.—Emergent X-ray continuum spectra as functions of orbital phase, ϕ. *Dashed curves*: spectra that would result if the wind were neutral.

and ionization state of the gas along the line of sight to the source. Since the inclination of the 4U 0900−40/HD 77581 binary system is close to 90° (Conti 1978), we shall neglect the distinction between the angle θ_0 between the line of centers and the ray to the observer and the orbital phase angle and approximate $\theta_0 = \pi(1 - 2\phi)$, where orbital phase $\phi = 0$ corresponds to the center of the X-ray eclipse. (The generalization to arbitrary orbital inclination is given by eq. [A1] in the Appendix.) Near X-ray eclipse the line of sight to the X-ray source traverses a large column density of stellar wind which is not highly ionized by X-rays. The dominant opacity above 1 keV is due to *K*-shell absorption by ions of C, N, and O, the cross sections of which are almost independent of the number of *L*-shell electrons, and the absorption spectrum closely resembles that of neutral gas (e.g., Brown and Gould 1970). For example, at orbital phase $\phi = 0.2$ the theoretical spectrum fits well with absorption by cold gas with column density $N = 3.1 \times 10^{22}$ cm^{-2} and agrees with the observed spectrum (Kallman and White 1982—but cf. § V). However, the X-ray opacity of the wind is reduced significantly in the regions where C, N, and O are fully ionized. This effect is illustrated by the dashed curves in Figure 3, which show the emergent spectra that would result if the wind were neutral. For example, at $\phi = 0.2$ the difference between the dashed curve and the solid curve corresponds to a reduction of column density of neutral gas by 40%.

X-rays can dramatically suppress the opacity at energies < 1 keV by photoionizing He II and all ions of C, N, and O with *L*-shell electrons. As implied by the results shown in Figures 2*a*–2*d*, soft X-rays can penetrate and ionize the lower gas densities at large distances from the primary, greatly reducing the soft X-ray opacity at the orbital phases farthest from eclipse. This effect is apparent in Figure 3 at $\phi = 0.5$, where $\sim 5\%$ of the incident intensity below 1 keV leaks out to large distances, and the spectrum shows dramatic departures from the simple cold gas absorption (*dashed curve*).

IV. P CYGNI LINE PROFILES

In an isolated OB star, ultraviolet resonance lines are formed largely by resonant scattering of stellar continuum photons by ions of trace elements in the stellar wind. A blueshifted absorption component results from scattering of photons out of the beam from the stellar disk to the observer by ions moving toward the observer. Superposed on the stellar continuum with this absorption feature is an emission line resulting from scattering of isotropic stellar continuum photons toward the observer by ions in the radially outflowing wind. Since the emission line is formed by ions in the far side of the stellar wind as well as those in the near side, the emission component is roughly symmetrical about the resonance wavelength (except that some of the redshifted emission is eclipsed by the primary). The superposition of absorption on the stellar continuum and emission results in a P Cygni type profile, with a strong absorption feature on the blue side of the resonance wavelength and a weaker emission feature on the red side.

Asymmetries in the distribution of ions in the stellar wind resulting from the action of a binary X-ray source will manifest themselves as variations in the profiles of the P Cygni lines with orbital phase. One can see qualitatively (Hatchett and McCray 1977) that if an ion responsible for a given resonance line is removed by X-ray photoionization from a region of stellar wind on the near side of the star, the blueshifted absorption will be suppressed. Conversely, if the abundance of an ion is increased on the near side, the absorption will be enhanced.

Quantitatively, P Cygni line profiles can be calculated by using the Sobolev approximation (Sobolev 1957, 1960; Castor 1970; Lucy 1971; Castor and Lamers 1979), which takes advantage of the fact that the line shapes are formed by gradients in the velocity fields of these very supersonic winds rather than by thermal Doppler motions. For a single resonance line, photons observed at a given wavelength are scattered only by gas within a narrow range of velocities, such that

$$\lambda = \lambda_0(1 - v_{\parallel}/c)\,, \tag{11}$$

where $v_{\parallel}$ is the component of wind velocity projected toward the observer. For monotonically accelerated winds the condition $v_{\parallel}$ = constant defines a unique surface in the wind, called the resonant surface. Figure 4 shows these surfaces for a wind whose velocity profile is given by equation (2).

We assume that the density and velocity structure of the wind are unaffected by the presence of the X-ray source, and that the ionization of the wind can be calculated quasi-statistically, i.e., assuming balance between ionization and recombination. As a result the wind ionization structure is axisymmetric with respect to the line of centers of the binary system, and the line profile that will be seen by an external observer depends only on the angle, θ_0, between the line of centers and the line of sight.

The flux in a resonance line at a given wavelength is calculated by integrating the specific intensity emerging from such a surface over a family of rays parallel to the line of sight:

$$L_\lambda = 4\pi \int_0^{2\pi} d\eta \int_0^{\infty} pdpI_\lambda(p, \eta)\,, \tag{12}$$

where p is the impact parameter of the ray with respect to the primary, and η is the azimuthal angle of the ray. The specific intensity has the form

$$I_\lambda(p, \eta) = \exp(-\tau_\lambda)I_c + [1 - \exp(-\tau_\lambda)]S_\lambda\,, \tag{13}$$

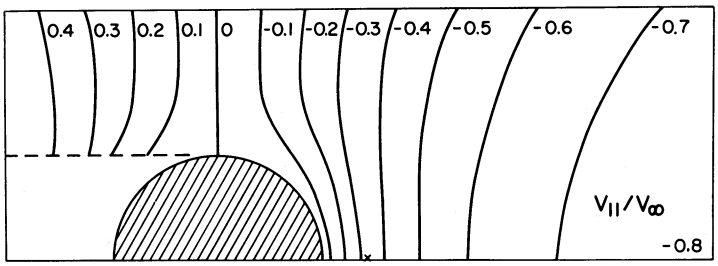

FIG. 4.—Contours of constant projected stellar wind velocity, $v_{\|}$, for the 4U 0900−40/HD 77581 system. The curves are labeled by the ratio $v_{\|}/v_{\infty} = \Delta\lambda/\Delta\lambda_T$.

where the line optical depth, τ_λ, and the source function, S_λ, are functions of the ion density, the radial and transverse velocity gradients of the wind at the resonant surface, and the angle, θ, between the line of sight and the radial direction at the resonant point. Expressions for these functions and details of our method of evaluating equation (12) are given in the Appendix. Note that I_λ does not have azimuthal symmetry unless the observer is viewing the binary system along its line of centers, because the X-ray photoionization breaks the spherical symmetry of the ion densities.

I_c is the intensity of the primary star's photosphere if the ray intersects the primary; otherwise it is zero. We have assumed that I_c is a flat continuum. There is no obstacle to including a photospheric line profile or limb darkening (which may be significant—cf. Castor and Lamers 1979), but for simplicity we have not done so. We normalize our emergent line fluxes, L_λ, to the emergent continuum flux, $L_c = 4\pi^2 R_*^2 I_c$, to yield the line profile.

Actually, the resonance lines considered are doublets, with the blue component having twice the oscillator strength of the red component. The doublet spacings are of the same order of magnitude as the Doppler shift corresponding to typical stellar wind velocities. This circumstance substantially complicates the calculation of the line profiles, because it becomes possible for a photon to be scattered first in the blue component of the resonance doublet and again, at another location, by the red component. We have neglected this effect and have calculated the line profiles as if they were single lines with the parameters of the blue component. At the end of this section we will discuss how we expect our results to be modified by the effects of the doublet separations.

In order to understand the line profiles, it is useful to refer to the hatched curves in Figures 2*a*–2*d* indicating the surfaces where the radial optical depth, $\tau_\lambda = 1$ (eq. [3]). Well inside these surfaces the wind is transparent to resonance scattering, negligible diffuse scattering of resonance lines into the beam occurs, and few resonance line photons are scattered out of the beam. Since every point in the wind corresponds to a unique wavelength in the resonance line, one can infer the wavelength range for which resonant scattering is suppressed or enhanced by X-ray ionization at phase $\phi = 0.5$ by superposing Figure 4 onto Figures 2*a*–2*d*, and at other phases by rotating Figure 4 through the corresponding angle and then superposing it on Figures 2*a*–2*d*.

For example, consider the phase dependence of the Si IV λ1394 line for our model of the 4U 0900−40/HD 77581 system, illustrated in Figure 5*a*. If there were no X-ray source in this system the theoretical Si IV line profile in this system would consist of the solid emission peak labeled $\phi = 0.5$ on the red side of the resonance wavelength and the dashed absorption trough labeled $\phi = 0$, 0.25 on the blue side. Figure 2*a* shows that the zone of transparency to resonance scattering fills most of the half-space on the side of the X-ray source, and the superposition of Figure 4 shows that this zone of transparency extends from $v_{\|}/v_{\infty} = -0.15$ to $v_{\|}/v_{\infty} = -1$. Therefore, when the X-ray source is on the near side of the star ($\phi = 0.5$), the absorption is completely removed for $\delta\lambda/\delta\lambda_T < -0.15$. The little peak at $\delta\lambda/\delta\lambda_T = 0.15$ is formed by forward scattering by Si IV ions at large distances on the near side. When the X-ray source is eclipsed ($\phi = 0$), Si IV is again present in front of the star and the absorption trough returns, but the redshifted wing of the emission is suppressed slightly as a result of the photoionization of Si IV on the far side of the star. Note that the absorption trough is unaffected by the X-ray source even at quadrature ($\phi = 0.25$) because the transparent zone does not occult the star.

The behavior of the C IV λ1548 resonance line (Fig. 5*b*) is similar, though less pronounced because the zone of transparency is smaller. (C IV is more durable than Si IV because of its higher ionization potential.) The surface for $\tau_\lambda = 1$ is open, but the surface for $\tau_\lambda = \frac{1}{2}$ (*dashed curve*) is closed and roughly equal in size to the primary star. If there were no X-ray source the line would consist of the solid redshifted emission profile and the dashed ($\phi = 0$) absorption trough. When the X-ray source is in front of the star ($\phi = 0.5$), the zone of transparency occults the star and the absorption is suppressed. This suppression is greatest for $\delta\lambda/\delta\lambda_T = -0.53$, corresponding to the Doppler shift where the zone of transparency has the greatest diameter. (Note that this blueshift is substantially greater than the value $\delta\lambda/\delta\lambda_T = -0.33$ corresponding to the wind velocity at the X-ray source.) However, when the orbital phase has changed by 30° ($\phi = 0.42$) the zone of transparency occults only part of the primary, and by 60° ($\phi = 0.33$) the absorption trough has returned completely. The zone of transparency is not large enough to cause a noticeable suppression of the redshifted emission at any phase.

In contrast, the absorption profiles of the N V λ1239 and the O VI λ1032 line are *enhanced* at $\phi = 0.5$ as a result of the enhancement of the abundances of these ions by X-ray ionization (Figs. 2*c* and 2*d*). In the absence of X-rays (on the eclipsed side) the wind becomes optically thin ($\tau_\lambda = 1$) at $R > 2.7R_*$ ($v > 1100$ km s^{-1}) for N V λ1239 (Fig. 2*c*) and at $R > 9R_*$ ($v > 1500$ km s^{-1}) for O VI λ1032. For each case the resonance line profile in the absence of X-ray photoionization would consist of the solid ($\phi = 0.5$) emission peak and the dashed ($\phi = 0$) absorption trough. Note that this profile is weaker for N V owing to the lower abundance of nitrogen. Consequently, the effects of X-ray photoionization are more pronounced for the N V line. The X-rays substantially increase the absorption at $\phi = 0.5$ and even at quadrature ($\phi = 0.25$), while they enhance the emission at X-ray eclipse ($\phi = 0$). The suppression of the N V absorption due to the transparent

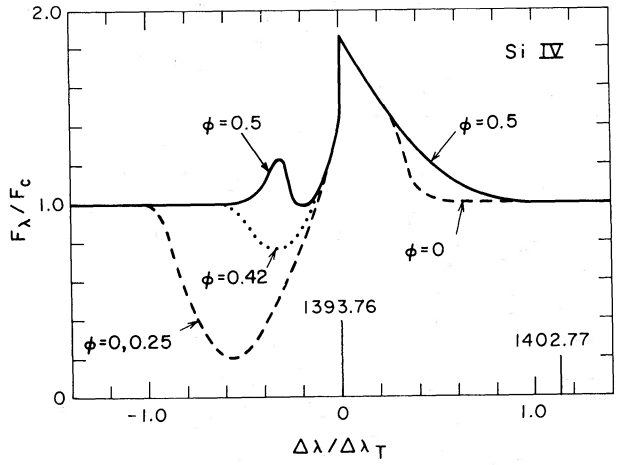

FIG. 5a

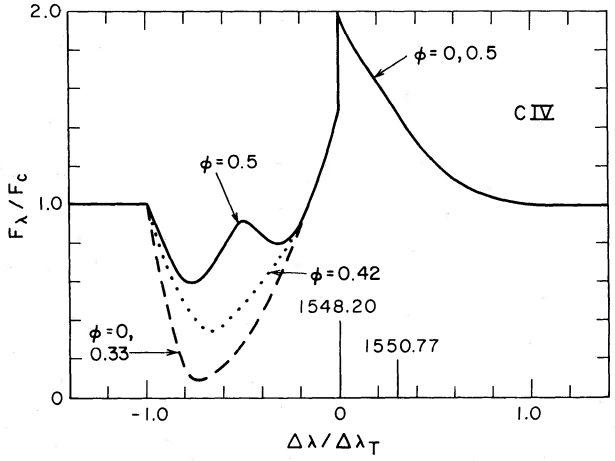

FIG. 5b

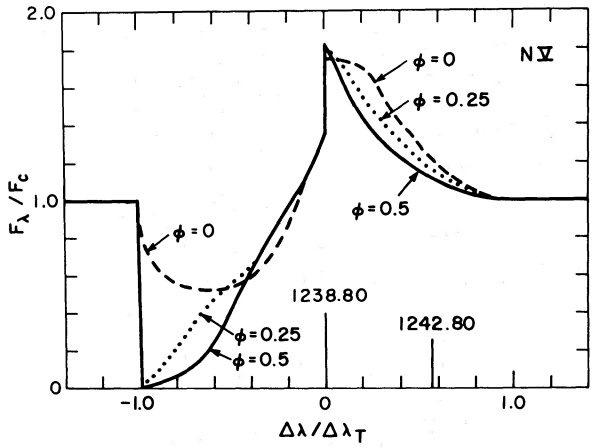

FIG. 5c

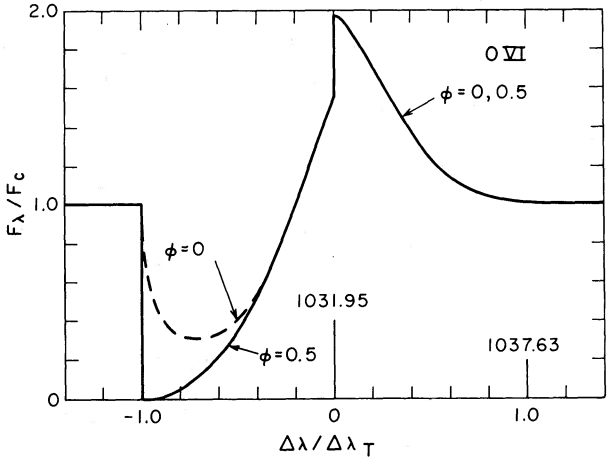

FIG. 5d

FIG. 5.—(*a*) Predicted profile of the Si IV λ1394 line as a function of orbital phase, φ, for the 4U 0900−40/HD 77581 system. Abscissa is line shift normalized to the maximum possible Doppler shift $\Delta\lambda_T = v_\infty/c$. Wavelengths and Doppler shifts of resonance doublets are indicated, assuming that the resonance wavelength is that of the stronger (blue) component and that $v_\infty = 1700$ km s^{-1}. (*b*) Same as Fig. 5*a* but for C IV λ1548. (*c*) Same as Fig. 5*a* but for N V λ1239. (*d*) Same as Fig. 5*a* but for O VI λ1032.

zone near the X-ray source is barely noticeable because this zone covers only a small fraction of the stellar disk. The effects of X-ray photoionization on the O VI line are similar, but less pronounced because the abundance of O VI without X-ray enhancement is high enough to make the line profile almost saturated at all wavelengths.

We now consider how these results should be modified to account for the doublet splitting of the resonance lines. The line splitting and wavelengths of the lines are indicated on Figures 5*a*–5*d* for each ion, assuming that $v_\infty = 1700$ km s^{-1}. Crudely, one can guess that the actual line profiles will be some sort of superposition of two such profiles, the stronger blue one shown centered at λ_B (where $\delta\lambda_B = 0$) and the weaker red one centered at λ_R; but the superposition is not linear. However, the profile of the blue component of the doublet will be unaffected by scattering in the red component for $\lambda < \lambda_R - \delta\lambda_T$. Thus, for example, in Si IV the predicted profile of the blue (1393.76 Å) component will be unaffected for $\lambda < 1394.87$ Å, or $\delta\lambda/\delta\lambda_T < 0.14$. However, for $0.14 < \delta\lambda/\delta\lambda_T < 1$ the red emission profile of the blue component will overlap with the blue absorption trough of the red component, and we cannot accurately predict how the profile should behave in this range without a more detailed calculation. The situation is qualitatively different for the case of C IV, where the doublet spacing is relatively small compared to $\delta\lambda_T$, and one can predict that the actual profile will behave roughly as a singlet, but smoothed out by $\delta\lambda = 2.50$ Å ($\delta\lambda/\delta\lambda_T = 0.28$). The worst case is that of N V, where the doublet spacing is comparable to the Doppler shift, $(\lambda_R - \lambda_B)/\delta\lambda_T = 0.57$, and the only part of the profile which can be predicted with confidence is the blue absorption wing for $\delta\lambda/\delta\lambda_T < -0.43$. The example of O VI is similar to that of Si IV, in that the doublet spacing is almost equal to the maximum Doppler shift, so that the predicted behavior of the absorption trough of the blue component should be unaffected by the line splitting.

V. DISCUSSION

For binary X-ray systems with early-type companion stars we have predicted that both the soft X-ray spectrum and the profiles of the ultraviolet resonance lines will vary with orbital phase as a result of photoabsorption of X-rays by ions in the stellar winds of the companion stars. Some of these effects,

such as the variable soft X-ray absorption and the suppression of the absorption troughs of the C IV λ1548 and Si IV λ1394 resonance lines by the X-ray source, have been observed in a number of such systems, including 4U 0900−40, SMC X-1, LMC X-4, and Cyg X-1. Other predictions, such as the enhancement of the absorption troughs of the N V λ1239 and O VI λ1032 resonance lines by the X-ray source, have not been observed yet. We now consider what can be learned about these and other such systems from comparison of the present theory with observations and from future improvements in theory and observations.

The theoretical models embody two main approximations. The first, that of neglecting the doublet separations in the calculations of the ultraviolet line profiles, is not a serious problem in principle. It can be removed by a straightforward, although technically complicated, extension of the present calculations. The second approximation, that of neglecting the effects of the X-ray source on the dynamics of the wind, presents a much more difficult and important problem. As discussed in § I, there are a number of ways in which the X-ray source can affect the wind, and none are understood well. Since we are not confident of our ability to calculate these effects from first principles, we consider the present theoretical calculations to provide only a qualitative guide to the observations. However, we hope that the theory will provide some insight into what the observations tell us about the actual dynamics of the winds.

We have modeled the best observed such system, 4U 0900−40/HD 77581. We have already mentioned in § III that the theoretical soft X-ray absorption spectrum agrees well with the observed spectrum at orbital phase $\phi = 0.2$, shortly after egress from eclipse. However, the observed soft X-ray spectrum does not vary with orbital phase in the way predicted by the model. In particular, the soft X-ray spectrum observed before ingress ($\phi = 0.8$) indicates a much greater column density of absorbing matter than that at egress (Kallman and White 1982). This observation clearly suggests some sort of density enhancement in the gas trailing the X-ray source. However, the structure of this density enhancement cannot be inferred from the X-ray observations alone. It might be a small density enhancement or gas stream near the X-ray source or a much larger wake in the wind. More detailed X-ray spectroscopic observations, with better coverage, will allow us to map the azimuthal distribution of column density in this structure, but they will not tell us its size.

The ultraviolet resonance line profiles are formed by structures in the ionization of the wind that are comparable in size to the companion star and the orbital separation. The absorption profiles of the Si IV and C IV are suppressed by about the amount predicted when 4U 0900−40 is in front of HD 77581, indicating ionization zones in the wind of about the size predicted by the theory. However, the profiles of the observed lines do not agree in detail with the theoretical ones. (This is sometimes true even for the resonance line profiles formed in the winds of single stars.) Some of the discrepancy might be attributed to our neglect of the doublet effect in the theory. For example, in C IV λ1548 the observed absorption trough at $\phi = 0.5$ is double, as predicted by theory, but the deeper absorption occurs at low velocity rather than at high velocity. This might be explained by the fact that both the 1548 Å and the 1551 Å components can contribute to the low-velocity feature, while only the 1548 Å component can contribute to the high-velocity feature. Some of the discrepancy might also arise from an unknown photospheric contribution to the resonance line.

Observations of the resonance absorption line profiles offer the opportunity to infer the size of the density structure in the wind that is responsible for the asymmetries in the orbital variations of the soft X-ray spectra. If this structure is comparable in size to HD 77581, asymmetries should also show up in the orbital variations of the ultraviolet lines; but if it is much smaller than HD 77581, it should not significantly affect the ultraviolet lines. It is possible, but not at all certain, that the large-scale density structure of the stellar wind is not affected much by the X-ray source. Abbott (1981) has suggested that the radiation force on the wind due to resonance scattering of stellar continuum photons should be fairly independent of the ionization state of the wind, because so many different ions and resonance lines can contribute to this force. If so, the dynamics of the stellar wind would be modified by X-ray photoionization and gravity only in a region very near the X-ray source, much smaller than the companion star.

We do not expect the red emission components of the P Cygni lines to provide very useful diagnostics of the X-ray influence on the wind, for three reasons. These are as follows. First, the emission component is built of small contributions from a region much larger than the O star, and therefore the effect of changing the ionization state in a moderate volume near the O star is small. Our calculations illustrate this. Second, we know from observations of single O stars that the emission components do not agree well with the profiles calculated by the Sobolev model in which a flat continuum is assumed for the O star's photosphere. The observed emission strength is often much less than that from the Sobolev calculation. This is not well understood; various possible explanations have been discussed by Abbott, Bohlin, and Savage (1982), of which the most likely is that the photospheric continuum is in reality a broad absorption feature. Third, the emission component is formed by scattering in both components of the doublet.

Although observations have demonstrated the possibility of using observations of compact X-ray binaries to probe stellar winds, the present data have serious limitations. In particular, the X-ray sources are known to vary intrinsically by large (>2) factors in time scales less than the orbital period. The resonance line profiles will vary as a result of these intrinsic X-ray luminosity variations. Therefore, simultaneous observations of both the X-ray spectra and the ultraviolet spectra as a function of orbital phase will be required in order to distinguish the effects of intrinsic X-ray variability from those of the changing orbital geometry. In addition, the present ultraviolet spectra, even for 4U 0900−40/HD 77581, the brightest such system, have inadequate phase coverage and signal-to-noise ratios to permit a detailed analysis of the ionization structure in the wind.

Finally, we comment on how the effects described here should depend on the parameters of other binary X-ray systems with early-type companion stars. The degree of ionization of trace elements in the wind is controlled largely by the parameter $\xi_0 = 4\pi\mu v(D)L_x/\dot{M}$. Thus, systems with more luminous X-ray sources or weaker winds than 4U 0900−40/HD 77581 will have relatively larger ionization zones, and their ultraviolet resonance lines should vary more dramatically. For example, in such systems the ionization zones of N V and O VI might be large enough to cause their resonance lines to vary in the same way as the Si IV and C IV lines do.

Similar orbital variations have been observed in the ultraviolet resonance lines from the early-type binary X-ray systems Cyg X-1 (Treves *et al.* 1980), SMC X-1 (Hammerschlag-Hensberge, Kallman, and Howarth 1984), and LMC X-4 (van der Klis *et al.* 1982). These systems do seem to have more luminous X-ray sources and weaker winds than 4U 0900−40/HD 77581, and their resonance lines behave roughly as expected. Unfortunately, these systems are so faint that the *IUE* spacecraft cannot obtain high-resolution ultraviolet spectra with good signal-to-noise ratios and phase coverage. Detailed theoretical models do not seem warranted by the presently available observations.

Good high-dispersion ultraviolet spectra have been obtained with *IUE* for the early-type binary system 4U 1700−37/HD 153919 (Dupree *et al.* 1978); they show no discernible variations of the Si IV, C IV, and N V resonance lines. This result can be understoos because the X-ray luminosity of this system is low and the stellar wind is strong, so that ξ_0 is small and the zones where the resonance line opacities are affected by X-ray photoionization are much smaller than the companion star. However, we predict dramatic orbital variations in the O VI λ1032 line in this system, since significant O VI line opacity can be produced by a small amount of X-ray illumination.

Another possible way to observe asymmetries in the distribution of ions in stellar winds is to measure linear polarization in the resonance line profiles. One can see qualitatively that the scattered radiation in the line should be linearly polarized with the electric vector parallel to the projected orbital axis when the X-ray source is displaced to either side of the companion star. Since the production of polarized photons by resonant scattering reaches a maximum when $\tau_\lambda \approx 1$ (Goldreich and Kylafis 1982), the polarization should show up best at those wavelengths in the line profile corresponding to projected wind velocities (Fig. 4) in the regions where $\tau_\lambda \approx 1$ (Figs. 2*a*–2*d*). Thus, we predict that the maximum in the linear polarization will appear first in the redshifted part of the line profile as (possibly before) the X-ray source emerges from eclipse and will move to shorter wavelengths, reaching its maximum degree for $\Delta\lambda = 0$ at $\phi = 0.25$, then move to the blue-shifted part of the profile. The polarization should vanish at $\phi = 0.5$, and the sequence should repeat in reverse as the source moves through $\phi = 0.75$. Although a detailed calculation is beyond the scope of this paper, we estimate that the linear polarization in the line profile may reach a few percent under optimal circumstances.

It should be possible to observe these and other such systems in much better detail with future instrumentation. The Space Telescope will be able to obtain excellent high dispersion ultraviolet line profiles and measure the polarization within them, and the *Advanced X-Ray Astronomy Facility* will be able to provide complementary X-ray spectroscopic observations. Such observations will be a powerful tool for exploring the dynamics of stellar winds and their interactions with compact X-ray sources.

This work was supported in part by grants from NASA (NSG-7128) and NSF (AST 80-19874) to the University of Colorado and by computing facilities provided by the National Center for Atmospheric Research, which is supported by the NSF.

APPENDIX

CALCULATION OF LINE PROFILES

The geometry used for our calculation is depicted in Figure 6, where R is the radial distance from the center of the primary (O) to the point P on the resonant surface; r is the radial distance from the secondary (X) to P; p is the impact parameter of the ray from P to Earth with respect to the ray from O to Earth; η is the azimuthal angle of the ray, θ_0 is the angle between the line of centers OX and the line of sight from O to Earth; θ is the angle between the radius vector to the resonant point OP

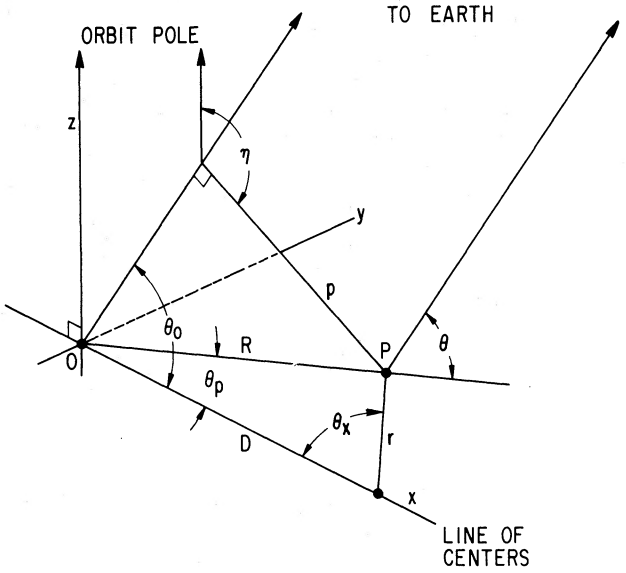

FIG. 6.—Binary system geometry. O is the location of the center of the primary, X is the center of the secondary, and P is the location of a parcel of stellar wind. The line of sight to O is not necessarily in the y, z plane.

and the line of sight from P to Earth; θ_p is the angle between OP and OX; and θ_x is the angle between OX and PX. We define the corresponding direction cosines: $\mu = \cos\theta$; $\mu_0 = \cos\theta_0$; $\mu_p = \cos\theta_p$; and $\mu_x = \cos\theta_x$. For arbitrary orbital inclination angle, i, we have the relation

$$\cos\theta_0 = -\sin i \cos 2\pi\phi \,. \tag{A1}$$

The line source function for the conservative scattering process that we assume is determined by the rate of scattering of continuum photons at that point, i.e.,

$$S = I_c \beta_c/\beta \,, \tag{A2}$$

in which the escape probability functions β and β_c (Castor 1970) are given by angle integrals involving the Sobolev optical depth for each direction at the resonant point:

$$\beta = \frac{1}{4\pi}\int \frac{1-e^{-\tau}}{\tau}\, d\Omega \,, \qquad \text{and} \qquad \beta_c = \frac{1}{4\pi}\int_c \frac{1-e^{-\tau}}{\tau}\, d\Omega \,. \tag{A3}$$

The integral for β_c is extended only over those directions that intersect the primary's photosphere.

The Sobolev optical depth, $\tau(\mu)$, is zero if the primary lies between the observer and the resonant point along the ray. Otherwise it depends on the line-of-sight velocity gradient, which in turn is a function of the local radial and transverse velocity gradients, μ, and the ion density at the resonant point. We have the relation

$$\tau = \tau_0/(1 + \sigma\mu^2) \,, \tag{A4}$$

in which τ_0 is the *transverse* optical depth and σ is the velocity gradient anisotropy factor defined by

$$\sigma = \frac{R}{v}\frac{dv}{dR} - 1 \,. \tag{A5}$$

The transverse optical depth τ_0 can be expressed in terms of the *radial* optical depth $\tau_{\rm rad}$ by

$$\tau_0 = \tau_{\rm rad}(1 + \sigma) \,. \tag{A6}$$

For the P Cygni lines that we are considering, the opacity is very nearly proportional to the total number of ions in question, since almost all such ions are in the ground state. If we designate by g_i the relevant ionization fraction and if, furthermore, g_i^0 is the corresponding ionization fraction in the absence of the X-ray source, then we can write

$$\tau_{\rm rad} = (g_i/g_i^0)\tau_{\rm rad}^0 \,, \tag{A7}$$

where $\tau_{\rm rad}^0$, the radial optical depth in the absence of the X-ray source, is given by equation (1) and the parameters listed in Table 1.

Our computational technique is the following: equations (12) and (13) are put in the form

$$\frac{L_\nu}{L_c} = 1 + \frac{1}{\pi}\int_{-1}^{1}(1-y^2)^{-1/2}dy\left[\int_0^1 (S-1)(1-e^{-\tau})2p\,dp + \int_0^1 2p^3 S(1-e^{-\tau})du\right] , \tag{A8}$$

in which we have defined $y = \cos\eta$ and $u = 1/p$. Note that $p^3S(1-e^{-\tau})$ tends to a finite limit as p becomes large and the frequency is held fixed. The integrals in equation (A8) are done using appropriate variations of Gaussian quadrature. There is reflection symmetry with respect to the plane of the line of sight and the line of centers, so the integration over η need only cover the range 0 to π ($y = -1$ to 1). For this integral we use Gauss-Chebyshev quadrature with 12 abscissae y_i. (This is the same as a trapezoidal rule vs. η in which use is made of the periodicity.) The integral over p from 0 to 1 is done with a 12 point Gauss-Jacobi quadrature, that is, the factor p in the integrand is included as a weight function. The u integral is done with standard 12 point Gaussian quadrature, transformed from the integral $(-1, 1)$ to the interval (0, 1). The points and weights for these schemes are given by Abramowitz and Stegun (1964, § 25.4).

Since the ionization has axial symmetry about the line of centers, q_i depends on R and μ_p. The interpolation of q_i/q_i^0 at the resonant point provides $\tau_{\rm rad}$ through equation (A7), and therefore also τ_0 through equation (A6). The functions β and β_c defined by equation (A3) depend on τ_0, σ, and $\mu_c = [1 - (1/R^2)]^{1/2}$, the cosine of the cone angle subtended by the primary. We calculate these using an approximation suggested by G. Rybicki (private communication). The source function S follows from equation (A2), the optical depth τ along the line of sight is given by equation (A4), and these are all the pieces needed to evaluate the integrals in equation (A8).

The calculation proceeds as follows. We define the dimensionless frequency variable,

$$\delta = -\frac{c}{v_\infty}\frac{\Delta\lambda}{\lambda_0} \,, \tag{A9}$$

so that $\delta = +1$ is the violet edge of the absorption trough in the P Cygni profile and $\delta = -1$ is the red edge of the emission component. We select values for δ and θ_0 (we choose multiples of 0.05 and 30°, respectively). For given δ and p we find the radius of the resonant point from

$$\delta = w(R)[1 - (p^2/R^2)]^{1/2} \tag{A10}$$

(radial dimensions are normalized to R_* and the terminal velocity has been set to unity). With the chosen velocity law (eq. [2]),

a nonlinear equation for R results, which is solved using the Newton-Raphson method. Having solved equation (A10) for the radius, the direction cosine μ follows from

$$\mu = \delta/w(R) \tag{A11}$$

The direction cosine μ_p then follows from the spherical law of cosines:

$$\mu_p = \mu_0 \mu + (1 - \mu_0^2)^{1/2}(1 - \mu^2)^{1/2} y \, . \tag{A12}$$

The coordinates R and μ_p locate the resonant point P with respect to the centers of the primary and secondary stars. Specifically, the polar coordinates of P with respect to the secondary (X) are

$$r = (R^2 + D^2 - 2RD\mu_p)^{1/2} \tag{A13}$$

and

$$\mu_x = (D - \mu_p R)/r \, . \tag{A14}$$

REFERENCES

Abbott, D. C. 1981, *Ap. J.*, **259**, 282.
Abbott, D. C., Bohlin, R. C., and Savage, B. D. 1982, *Ap. J. Suppl.*, **48**, 369.
Abramowitz, M., and Stegun, I. 1964, *Handbook of Mathematical Functions* (Washington, D.C.: U.S. Department of Commerce).
Becker, R. H., *et al.* 1978, *Ap. J.*, **221**, 912.
Brown, R. L., and Gould, R. J. 1970, *Phys. Rev. D.*, **1**, 2252.
Buff, J., and McCray, R. 1974, *Ap. J. (Letters)*, **188**, L37.
Cassinelli, J., and Olson, G. L. 1979, *Ap. J.*, **229**, 304.
Castor, J. I. 1970, *M.N.R.A.S.*, **149**, 111.
Castor, J. I., and Lamers, H. J. G. L. M. 1979, *Ap. J. Suppl.*, **39**, 481.
Conti, P. S. 1978, *Astr. Ap.*, **63**, 295.
Conti, P. S., and McCray, R. 1980, *Science*, **208**, 9.
Dupree, A. K., *et al.* 1978, *Nature*, **275**, 400.
———. 1980, *Ap. J.*, **238**, 969.
Fransson, C., and Fabian, A. C. 1980, *Astr. Ap.*, **87**, 102.
Friend, D. B., and Castor, J. I. 1982, *Ap. J.*, **261**, 293.
Gathier, R., Lamers, H. J. G. L. M., and Snow, T. P. 1981, *Ap. J.*, **247**, 173.
Goldreich, P., and Kylafis, N. D. 1982, *Ap. J.*, **256**, 606.
Hammerschlag-Hensberge, G., *et al.* 1980, *Astr. Ap.*, **85**, 119.
Hammerschlag-Hensberge, G., Kallman, T. R., and Howarth, I. D. 1984, *Ap. J.*, in press.
Hatchett, S., and McCray, R. 1977, *Ap. J.*, **211**, 552.
Kallman, T., and McCray, R. 1982, *Ap. J. Suppl.*, **50**, 263.
Kallman, T. R., and White, N. E. 1982, *Ap. J. (Letters)*, **261**, L35.
Klein, R. I., and Castor, J. I. 1978, *Ap. J.*, **220**, 902.
Lucy, L. B. 1971, *Ap. J.*, **163**, 95.
Lucy, L. B., and White, R. L. 1980, *Ap. J.*, **241**, 300.
MacGregor, K., and Vitello, P. 1982, *Ap. J.*, **259**, 267.
Olson, G. L. 1978, *Ap. J.*, **226**, 124.
Olson, G. L., and Castor, J. I. 1981, *Ap. J.*, **244**, 179.
Sobolev, V. V. 1957, *Soviet Astr.–A.J.*, **1**, 678.
———. 1960, *Moving Envelopes of Stars* (Cambridge, Mass.: Harvard University Press); Russian edition 1947.
Tarter, C. B., Tucker, W., and Salpeter, E. E. 1969, *Ap. J.*, **156**, 943.
Treves, A., *et al.* 1980, *Ap. J.*, **242**, 1114.
van der Klis, M., *et al.* 1982, *Astr. Ap.*, **106**, 339.

JOHN I. CASTOR: Lawrence Livermore Laboratory L-18, P.O. Box 808, Livermore, CA 94550

TIMOTHY R. KALLMAN: Code 665, NASA/Goddard Space Flight Center, Greenbelt, MD 20771

RICHARD MCCRAY: JILA, University of Colorado, Boulder, CO 80309

GORDON L. OLSON: 470 Aragon, White Rock, NM 87544